MiR-21 deficiency alters the survival of Ly-6C^{lo} monocytes in *ApoE*$^{-/-}$ mice and reduces early-stage atherosclerosis

Anna Chipont (MS)[1], Bruno Esposito (BS)[1], Inès Challier (MS)[1], Mélanie Montabord (MS)[1], Alain Tedgui (PhD)[1], Ziad Mallat(MD, PhD)[1], Xavier Loyer (PhD)[1], Stephane Potteaux (PhD)[1]

[1]INSERM U970, PARCC, 56 rue Leblanc, 75015 Paris

Running title: Role of miR-21 in experimental atherosclerosis

Corresponding Author: Stephane Potteaux, UMR970, PARCC, 56 rue Leblanc, 75015 Paris

Subject codes: Atherosclerosis, Basic Science Research, Inflammation

Word count: 5883

Two figures and ten supplemental figures

Abstract

OBJECTIVE :
To determine the role of miR-21 on the homeostasis of monocyte subsets and on atherosclerosis development in *ApoE*$^{-/-}$ mice.
APPROACH and RESULTS :
In *ApoE*$^{-/-}$ mice, miR-21 expression was increased in circulating Ly-6C^{lo} monocytes (NC-Mo) in comparison to Ly-6C^{hi} monocytes. The absence of miR-21 significantly altered the survival and number of circulating NC-Mo in *ApoE*$^{-/-}$ mice. In the early stages of atherosclerosis, the absence of miR-21 limited lesion development both in the aortic sinus (by almost 30%) and in the aorta (by almost 50%). This was associated with less monocyte availability in circulation and increased apoptosis of local macrophages in plaques. At later stages of atherosclerosis, lesion size in the aortic root was similar in *ApoE*$^{-/-}$ and *ApoE*$^{-/-}$*miR-21*$^{-/-}$ mice, but plaques showed a less stable phenotype (larger necrotic cores) in the latter. The loss of protection in advanced stages was most likely due to excessive inflammatory apoptosis related to an impairment of local efficient efferocytosis.
CONCLUSION : Gene deletion of miR-21 in *ApoE*$^{-/-}$ mice alters NC-Mo homeostasis and contribute to limit early-stage atherosclerosis.

Non standard Abbreviations and acronyms:
C-Mo : Ly-6C^{hi} classical monocytes
NC-Mo : Ly-6C^{lo} nonclassical monocytes
ApoE : Apolipoprotein E
Ldlr : Low density lipoprotein receptor
BMT: Bone marrow transplantation

Introduction

Monocytes are critical to the development of atherosclerosis and inhibition of monocyte development or trafficking strongly impairs atherosclerotic lesion formation[1-3]. Monocyte-derived macrophages accumulate in the plaque and transform into lipid-loaded foam cells, often committed to death. In early plaques, when phagocytic clearance of apoptotic cells (efferocytosis) is optimal, apoptosis is beneficial and helps limit lesion development. In the later stages of atherosclerosis, when efferocytosis is deregulated, necrosis secondary to apoptosis promotes plaque inflammation and lesion progression[4]. Currently, several types of monocyte subsets have been described and are thought to have divergent functions. In mice, classical Ly-6C^{hi}CCR2^{+} monocytes (C-Mo) migrate to sites of injury where they differentiate into inflammatory macrophages. C-Mo dominate hypercholesterolemia-associated monocytosis and macrophage accumulation in the plaque[5]. In contrast, Ly-6C^{lo}CX3CR1^{hi} non-classical monocytes (NC-Mo) exhibit a unique ability to patrol the vasculature and remove damaged cells and debris[6]. In atherosclerosis, the exact role of NC-Mo is not fully understood. Recent studies suggested that their patrolling along the vascular wall limit vascular inflammation and early atherogenesis[7, 8]. The transcription factor NR4A1 is absolutely required for NC-Mo development, and mice deficient for *NR4A1* lack NC-Mo and accumulate M1-like macrophages in the plaque, favoring accelerated atherosclerosis[9]. However, in another study, the lack of *NR4A1* had no impact on macrophage polarization and did not change atherosclerosis[10]. More recently, E2 domain-deficient *Ldlr*$^{-/-}$ mice which lack Ly6C^{low} monocytes but retain *Nr4a1* gene expression in macrophages were shown to have accelerated atherosclerosis[8]. The chemokine receptor CX3CR1 also contribute to NC-Mo survival and the absence of CX3CR1, which impairs NC-Mo number in blood of *ApoE*$^{-/-}$ or *Ldlr*$^{-/-}$ mice, protected mice against atherosclerosis[11, 12]. The discrepancy between these studies highlights the need to identify key molecular mechanisms underlying maintenance of monocyte subsets. MicroRNAs are well-conserved, short non-coding RNAs, known to play major roles in most biological processes by influencing the stability and translation of mRNAs[13].

miR-21 plays important roles in leukocyte function, driving both cell polarization and survival, particularly during inflammatory conditions[14-16]. miR-21 has been linked to several cardiovascular diseases and highly correlates with the evolution of multiple cancers. A recent study reported that deletion of miR-21 in the hematopoietic compartment of *LDLr*$^{-/-}$ mice on high fat diet (HFD) accelerated the development of advanced atherosclerosis in part through accumulation of inflammatory macrophages and defective efferocytosis[17]. Here, we aimed to investigate the role of miR-21 on homeostasis of monocytes in *ApoE*$^{-/-}$ mice and its effect in early and advanced stages of atherosclerosis.

Materials and Methods

All supporting data are available within the article [and its online supplementary files].

Animals

Experiments were conducted according to the guidelines formulated by the European Community for experimental animal use (L358-86/609EEC) and were approved by the Ethical Committee of INSERM and the French Ministry of Agriculture (agreement A75-15-32).
miR-21$^{-/-}$ mice were obtained from Pr. Marc E. Rothenberg (Cincinnati Children's Hospital Medical Center). *ApoE*$^{-/-}$ mice were from Jackson laboratories and are maintained in our animal

facility. *ApoE$^{-/-}$ miR21$^{-/-}$* mice were generated in our facility, and littermates *ApoE$^{-/-}$miR21$^{+/+}$ (called ApoE$^{-/-}$)* of the same age and sex were used as control. Because sexual dimorphisms have been reported in atherosclerosis studies[18], particularly when comparing early and advanced atherosclerosis[19], we used one gender to minimize the number of mice used in the study and chose males as in Canfran-Duque et al[17] and Jin et al[20]. B6-Ly5.1/Cr mouse, which carry the allele CD45.1 were purchased from Charles River and crossed to *ApoE$^{-/-}$* mice to generate *ApoE$^{-/-}$ CD45.1* mice. All mice used in these experiments were bred and housed in a specific pathogen-free barrier facility. Mice were either maintained on chow diet or put on a pro-atherogenic high fat diet (15% FAT, 1.25% cholesterol) as mentioned in the figure legends.

Flow cytometry and cell sorting assessment

Total blood has been collected on heparin or EDTA tubes before counting and staining. Mice were perfused with PBS before organ removal. The spleen was dissociated and the bone marrow flushed. Cells were filtered and counted before staining.

Blocking of non-specific binding of immunoglobulin to Fc receptors was done with a purified anti-mouse CD16/32 antibody. Leukocyte population was identified using the following antibodies: anti-CD11b (M1/70), anti-CD115 (AFS98), anti-Gr1 (RB6-8C5), anti-CD4 (RM4-5), anti-CD3 (145-2C11), anti-CD8 (53-6.7), anti-CD62L (MEL-14), Anti-CD44 (IM7) anti-B220 (RA3-6B2) and anti-NK1.1 (PK136). Chemokines receptors were stained using an anti-CCR2 (FAB5538P) and anti-CX3CR1 (SA011F11). We use anti-Bcl2 (Miltenyi Ref 130-105-430), anti-Ki67 (BD Pharmingen Ref 556027) and anti-P38 MAP Kinase (Thr180/Tyr182-Cell signaling). For M1 and M2 markers, we used an anti-CD206 (C068C2) and anti-MHCII (M5/114.15.2). Blood samples were lysed with Red Blood Cells Lysing Buffer (Sigma-Aldrich, USA) and washed twice before analysis. All samples were analyzed on LSR Fortessa Analyser, and datas were obtained with the FlowJo Software.

For cell sorting, the blood has been incubated with the following antibodies: anti-CD11b (M1/70), anti-Ly6C (AL-21), anti-Ly6G (1A8), anti-CD115 (AFS98), anti-CD19 (1D3), anti-CD4 (RM4), anti-CD8 (53-6.7). Samples were lysed with Red Blood Cells Lysing Buffer (Sigma-Aldrich, USA) then washed and ressuspended in PBS 1X for analysis on ARIA II SORP CELL SORTER. Samples were collected apart on Qiazol Reagent (Qiagen, Deutchland) and frozen at -80°.

mRNA analysis and real time qPCR

RNA from high and low monocytes were isolated using the RNeasy MicroKit (Qiagen, Deutchland) according to the manufacturer's instructions and frozen at -80°.

For the miRNA reverse transcription, 5ng/µL of isolated RNA were used with the miRCURY™ LNA™ Universal RT microRNA PCR (Exiqon A/S, Denmark). Real time quantitative polymerase chain reaction was performed with SYBER GREEN reagent (Eurogentec), using miR-21-5p and miR-21-3p (Exiqon A/S, Denmark) primer. miR-21 expression was normalized to U6, 5S and RNU5G (Exiqon A/S, Denmark) genes as references. Analysis was runned with ABI PRISM thermocycler. Relative expression was calculated using the 2-delta-delta CT method followed by geometric average, as recommended[21].

For the total mRNA reverse transcription, 100ng/µL of isolated RNA were used with the QuantiNova Reverse Transcription Kit (Qiagen, Deutchland). Real time quantitative polymerase chain reaction was operated with SYBER GREEN Reagent, using the following mouse primers: CX3CR1 5'-*GGAGTCTGCGTGAGACTGGGTGAGTGA*-3' and 5'-*GAGGGCGTAGAAGACGGACAGGAAGATG*-3',

Nur77 5'-*GTCCTGGAGCCCGTGTCGATCA*-3' and 5'-*TTCCCGCCTTTGCCTGCCTGT*-3', CCR2 5'-*GCCGTGGATGAACTGAGGTAACA*-3' and 5'-*GAGGGCATTGGATTCACCACA*-3', CCR5 5'-*GGCAGGAGCTGAGCCGCAATTTGTTT*-3' and 5'-*GGTGAGACATCCGTTCCCCCTACAAGA*-3', CXCR4 5'-*CTGAGGCGTTTGGTGCTCCGGTAA*-3' and 5'-*ATCCCGGAAGCAGGGTTCCTTGT*-3'. Relative expression of these genes were calculated using the ΔΔCT method, using the GAPDH 5'-*CGTCCCGTAGACAAAATGGTGAA*-3' and 5'*GCCGTGAGTGGAGTCATACTGGAACA*-3' as reference gene.

Bone marrow-derived macrophages and apoptosis assay *in vitro*

Primary macrophages were derived from mouse bone marrow-derived cells (BMDM). Tibias and femurs of mice were dissected and their marrow flushed out. Cells were grown for 7 days at 37°C in a solution of RPMI 1640 medium, 20% neonatal calf serum, and 20% macrophage–colony-stimulating factor-rich L929-conditioned medium. To analyze apoptosis susceptibility, untreated BMDM were incubated with fetal calf serum- free medium, TNF-α (10 μg/ml) and cycloheximide (10 μM), or etoposide (50 μg/ml) for 12 hours. Apoptosis was determined by using Annexin V fuorescein isothiocyanate apoptosis detection kit with 7-AAD (APC, BD Biosciences, San Jose, California) according to the manufacturer's instructions.

Dil^{+} liposome injection and monitoring of Ly-6C^{lo} monocyte *in vivo*.

Injection of Dil^{+} liposomes was used to address the role of miR-21 on the survival of NC-Mo *in vivo.* 200μl of fluorescent Dil liposomes (Clodronate Liposome) were injected intraveneously to *ApoE$^{-/-}$ and ApoE$^{-/-}$miR21$^{-/-}$* to label NC-Mo. About 50% of NC-Mo were labeled after 24 hours in both groups. The turnover of labeled NC-Mo was determined by flow cytometry at days 1, 4, 7 and 10 on 50μl of blood samples.

Bone marrow transplantation (BMT)

For the competition assay

8-week-old male *Apoe$^{-/-}$ CD45.2* mice were lethally irradiated (9.5 Gray) and intraveneously reconstituted with ten million cells coming from a 1:1 bone marrow cell mix of *ApoE$^{-/-}$* CD45.1 and *ApoE$^{-/-}$ miR21$^{-/-}$ (or ApoE$^{-/-}$ miR21$^{+/+}$* as control*)* CD45.2 medullar cells. Height weeks after reconstitution, blood samples were taken from mice maintained under isoflurane anesthesia to test the chimerism*.*

For atherosclerosis quantification

8 week-old male *Apoe$^{-/-}$* mice were lethally irradiated (9.5 Gray) and intraveneously reconstituted with ten million cells coming from *Apoe$^{-/-}$* or *Apoe$^{-/-}$miR-21$^{-/-}$* mice. Mice were kept on chow diet for 12 weeks post BMT or transitioned 4 weeks post BMT to a HFD for 10 weeks.

Quantification of atherosclerotic lesions

Mice were anesthetized with isoflurane before sacrifice. Plasma cholesterol was measured using a commercial kit (DiaSys® Cholesterol FS*, Germany). Quantification of lesion size and composition was performed as previously described[22] and is in agreement with the recent recommendation[23]. Briefly, the heart and ascending aorta were removed, perfusion-fixed *in situ* with 4% paraformaldehyde, then placed in phosphate-buffered saline (PBS)-30% sucrose solution overnight, before being embedded in frozen optimal cutting temperature compound and frozen at -70°C. Afterwards, 10-mm serial sections of aortic sinus were obtained (cut on cryostat). Lipids were detected using Oil Red O (Sigma-Aldrich, St. Louis, Missouri) coloration

and quantified by a blinded operator using HistoLab software (Microvisions Instruments, Paris, France) 30, which was also used for morphometric studies. For lesion size quantification, multiple sections in multiple regions were analyzed. For tissue characteristics, same regions of the aortic sinus were used between animals. En face quantification was used for atherosclerotic plaques along thoraco-abdominal aorta, as previously described [22].
Collagen was detected using Sirius red staining. The presence of macrophages was determined using monoclonal rat anti-mouse macrophage/monocyte antibody (MOMA)-2 (MAB1852). Apoptotic macrophages in the lesion were identified as MOMA-2$^+$ TUNEL$^+$ (Roche) or as cleaved-caspase 3$^+$ (5A1E). CD206 and MHCII stainings were done with anti-CD206 (C068C2) and anti-MHCII (M5/114.15.2) antibodies.

At least 4 sections per mouse were examined for each immunostaining, and appropriate negative controls were used.

Monocyte labeling *in vivo*. NC-Mo were labeled *in vivo* by retro-orbital i.v. injection of 1 µm fluorescent microsphere (YG, Polysciences) diluted 1/4 in sterile PBS. Cell labeling was checked 24 hours later by flow cytometry. The recruitment of bead$^+$ labeled NC-Mo was quantified in the aorta, 5 days after labeling by counting the number of beads in the digested aorta, by flow cytometry. For staining on aortic cells, the aorta was removed and flushed intensively with 2 mM 0,2% FBS PBS. The aorta was cut into pieces and digested using a cocktail of enzymes for 45 min at 37°C (450 U/ml collagenase I, 125 U/ml collagenase XI, 60 U/ml hyaluronidase I; all from Sigma-Aldrich).

Thioglycollate assay
Mice were injected intraperitoneally with 1 ml 3% thioglycollate. Peritoneal cells were harvested by successive lavages with cold PBS EDTA 0.5µM.

Efferocytosis assay *in vivo*
5 males *miR21*$^{+/+}$ and 5 males *miR21*$^{-/-}$ of 8 weeks were injected intraperitoneally with 2ml of 3% thioglycollate. 48 hours after, thymocytes from 4 weeks old C57Bl6 male mice were isolated, stained with CFSE (5µM) for 5 minutes at 37 degrees. The reaction was stopped by adding cold fetal calf serum and washed twice with steril PBS. Apoptosis of thymocytes was induced by exposing the cells to UV radiation (0.25 Joule/minute) for 10 minutes. Apoptosis was controlled by flow cytometry (Annexin V-7AAD staining). Ten millions apoptotic thymocytes were injected intraperitoneally (1ml) to mice treated with thioglycollate. After 1 hour, we collected the peritoneal macrophages by lavage and immediately fixed the cells in PFA 4% to stop the efferocytosis process. Macrophages were stained with CD11b, F4/80 and analyzed by flow cytometry. Macrophages that had engulfed CFSE+ apoptotic thymocytes were identified as follow: CD11b$^+$, F4/80$^+$, CSFE$^+$.

Statistical analysis.
Values are expressed as mean +/- SEM. Differences between values were evaluated using non-parametric Mann-Whitney test, or other as specified in the legends. All these analyses were performed using GraphPad Prism version 5.0b for Mac (GraphPad Software) and values were considered significant at $P<0.05$.

Results

miR-21 controls the maintenance and survival of NC-Mo in *ApoE*$^{-/-}$ mice

We generated *ApoE*$^{-/-}$*miR-21*$^{-/-}$ and *ApoE*$^{-/-}$*miR-21*$^{+/+}$ littermate controls. Under chow diet, plasma cholesterol levels were similar in the two groups (4.43 g/L ±2.53 in *ApoE*$^{-/-}$*miR-21*$^{-/-}$ mice versus 4.11 g/L ±1.02 in *ApoE*$^{-/-}$ mice, n=8-12/group). Likewise, the leukocyte populations in blood were mostly similar between the two groups, except for NC-Mo, which were decreased both in percentage and number, in the absence of miR-21 (Figure 1A and Figure I in the online-only Data Supplement). Similar observations were made in *ApoE*$^{+/+}$ *miR-21*$^{-/-}$ mice supplemented with a HFD (Figure II in the online-only Data Supplement). The defect in NC-Mo in *ApoE*$^{-/-}$*miR-21*$^{-/-}$ was seen in the spleen as well as in the bone marrow, revealing a general defect in NC-Mo production or maintenance (Figure IIIA and IIIB in the online-only Data Supplement). We therefore examined the expression level of miR-21 in circulating leukocytes. In *ApoE*$^{-/-}$ mice on chow diet, mir-21-5p was expressed at similar levels in monocytes, neutrophils, B and T cells (Figure IIIC in the online-only Data Supplement). Interestingly, its expression was 4-fold higher in NC-Mo compared to C-Mo (Figure 1B), suggesting that miR-21-5p might differently control the homeostasis of monocyte subsets. In contrast, miR-21-3p expression was bellow detection in all other circulating leukocyte subsets (not shown).

We investigated the impact of miR-21 in monocyte subsets by exploring the expression of genes involved in cell survival and migration. In absence of miR-21, NC-Mo showed decreased *Nr4a1* and *Cx3cr1* mRNA expression (Figure 1C) and decreased CX3CR1 protein level (Figure IVA in the online-only Data Supplement). In contrast, there was no change in *Ccr2* and *Ccr5* expression (Figure IVB in the online-only Data Supplement). We also observed a decrease in Ki67^{+} and BCL2^{+} NC-Mo in spleens of mice deficient for miR-21 (Figure 1D). miR-21 deficiency was associated with increased Phospho-P38 mitogen-activated protein kinase and decreased CD115 expression in circulating NC-Mo, but not in C-Mo (Figure 1D and Figure IVC in the online-only Data Supplement). These phenotypic changes suggest that miR-21 may be acting as a survival and/or differentiation factor in NC-Mo by promoting expression of factors important for monocyte function.

We therefore addressed the role of miR-21 on the homeostasis of NC-Mo *in vivo*. We pulse-labeled circulating NC-Mo with Dil^{+} liposomes and quantified their rate of disappearance in blood. Injected Dil^{+} liposomes exclusively labeled NC-Mo (not shown). In control *ApoE*$^{-/-}$ mice, the level of Dil^{+}NC-Mo decreased by 30% within 7 days. In contrast, *ApoE*$^{-/-}$*miR-21*$^{-/-}$ labeled NC-Mo decreased by 70% within 7 days, showing a higher rate of disappearance from blood (Figure 1E).

To complement this experiment, we designed a competitive congenic bone marrow (BM) transplant model, where irradiated *ApoE*$^{-/-}$*CD45.2* host mice were reconstituted with a 1:1 BM mix from *ApoE*$^{-/-}$*CD45.1* and *ApoE*$^{-/-}$*miR-21*$^{-/-}$*CD45.2 (*or control *ApoE*$^{-/-}$*CD45.2)* donors, enabling the independent tracking of reconstituted haematopoietic cells from each donor (Figure 1F). After transplantation, we found similar amounts of CD45.1 and CD45.2 leukocytes in the control group, showing no bias in CD45.1 versus CD45.2 cell reconstitution. In contrast, we observed a significant failure in the reconstitution of *miR-21*$^{-/-}$*CD45.2* compared to *CD45.1* cells in blood, revealing a bias in favor of miR-21 expressing cells. While the absence of miR-21 slightly affected every leukocyte subsets in blood, the proportion of *miR-21*$^{-/-}$ NC-Mo almost completely disappeared from the bloodstream (Figure 1F and Figure IVD in the online-only Data Supplement). These data confirmed that miR-21 deficiency controls monocyte subset ratios by

strongly impairing NC-Mo homeostasis in *ApoE*$^{-/-}$ mice, and revealed a more general effect of miR-21 on all leukocyte populations.

miR-21 deficiency transiently delays the development of atherosclerosis in *ApoE*$^{-/-}$ mice

We then explored the role of miR-21 at various stages of atherosclerosis development in *ApoE*$^{-/-}$ mice. In early atherosclerosis, at 10 weeks of age, the absence of miR-21 had no major impact on atherosclerosis lesion development or composition in *ApoE*$^{-/-}$ mice **(**Figure VA and VB in the online-only Data Supplement). At 24 weeks of age, the absence of miR-21 reduced atherosclerotic lesion size, both in the thoracic aorta and the aortic root (Figure 2A and 2B). In absence of miR-21, macrophage content was unchanged (Figure 2C), but the amount of TUNEL^{+} apoptotic macrophages was increased in lesions (Figure 2D). At this stage, smooth muscle cell accumulation and necrotic area extent were not altered (not shown). *In vitro*, we found that the lack of miR-21 increased the susceptibility of macrophages to apoptosis (Figure VIA in the online-only Data Supplement), which substantiates our *in vivo* data. In addition, we found that *miR-21*$^{-/-}$ macrophages became more inflammatory in plaques, as evidenced by the changes in CD206 and iNOS expression (Figure 2E). We confirmed that the absence of miR-21 broadly polarized macrophages to an M1-like signature (CD206^{-} MHCII^{hi}) **(**Figure VIB in the online-only Data Supplement). We also examined the role of miR-21 on monocyte migration *in vivo*. C-Mo recruitment was tested in a model of sterile peritonitis in the mixed BM chimeras presented in Figure 1F. We found similar chimerism of monocytes/macrophages in the blood before and in the peritoneum after thioglycollate injection, suggesting that the absence of miR-21 had no impact on C-Mo trafficking *in vivo* (Figure VIIA in the online-only Data Supplement). The recruitment of NC-Mo was quantified in the atherosclerotic aorta with a pulse-labeling method[24]. We found a decrease of bead^{+} NC-Mo in the aorta of mice deficient for miR-21 (Figure 2F), which could most likely be attributed to less NC-Mo in blood. Altogether, these data show that miR-21 deficiency decreases NC-Mo availability in blood, orientates plaque macrophages toward an inflammatory profile but increases their susceptibly to apoptosis. These concomitant events limit early atherosclerosis formation in *ApoE*$^{-/-}$*miR-21*$^{-/-}$ mice.

We next analyzed the role of miR-21 in advanced atherosclerosis by feeding mice a HFD for 10 weeks. miR-21-5p was expressed in all leukocyte subsets, independently of the diet. Again, its expression was increased in NC-Mo in comparison to C-Mo (Figure VIIB and VIIC in the online-only Data Supplement). miR-21 absence decreased the numbers of circulating NC-Mo (Figure VIIIA in the online-only Data Supplement) while not affecting total cholesterol levels (not shown). Despite a conserved protection in the aorta (Figure VIIIB in the online-only Data Supplement)**,** lesion size in the aortic root of *ApoE*$^{-/-}$*miR21*$^{-/-}$ was similar to control *ApoE*$^{-/-}$ mice (Figure VIIIC in the online-only Data Supplement). Macrophage content did not change, but the necrotic core area was increased in mice deficient for miR-21 (Figure VIIID and VIIIE in the online-only Data Supplement)**.** The amount of TUNEL^{+} apoptotic macrophages in lesions was increased and similar data were obtained using activated caspase-3 as an assay for lesional apoptosis (Figure IXA in the online-only Data Supplement). Neutral lipid and collagen contents were unchanged (Figure IXB in the online-only Data Supplement). Because necrotic core development likely occurs through the combination of defective efferocytosis and enhanced macrophage death, we examined the role of miR-21 on efferocytosis *in vivo*. The absence of miR-21 decreased by almost 2 fold the capacity of peritoneal macrophages to engulf CFSE-labelled apoptotic thymocytes (Figure 2G), in agreement with recent findings[18].

We additionally examined the specific contribution of myeloid-derived miR-21 in atherosclerosis development by performing bone marrow transplantations (BMT). The absence of miR-21 in the hematopoietic compartment reduced plaque size when mice were kept on chow diet for 12 weeks after BMT (Figure 2H), but had no effect when mice were fed a HFD for 10 weeks after BMT (Figure XA in the online-only Data Supplement)**.** As expected, the level of blood NC-Mo was decreased (Figure XB in the online-only Data Supplement). These results strengthen our conclusion that miR-21 deficiency impacts NC-Mo homeostasis, which at least in part contributes to limit early-stage atherosclerosis.

Discussion

The purpose of this study was to investigate the role of miR-21 in homeostasis of monocytes in *ApoE*$^{-/-}$ mice. RNA-based therapeutics have demonstrated great promise for the treatment of different diseases and miR-21 is an interesting target as it regulates macrophage polarization, apoptosis and efferocytosis[15]. Here, we report for the first time that miR-21 expression is increased in circulating NC-Mo from *ApoE*$^{-/-}$ mice on chow or high fat diet, compared to C-Mo. miR-21 deficiency in *ApoE*$^{-/-}$ mice significantly altered the amount of circulating NC-Mo, which could be accounted for by decreased NC-Mo longevity as shown by our *in vivo* experiments. We analyzed the role of miR-21 on atherosclerosis development in *ApoE*$^{-/-}$ mice, at 3 different stages of the disease. miR-21 deficiency partially protected against early development of atherosclerosis (at 10 and 24 weeks of age), despite the tendency of plaque macrophages to be more inflammatory and more susceptible to apoptosis. In contrast, at later stages of atherosclerosis (after 10 weeks on HFD), lesion size in the aortic root was similar in *ApoE*$^{-/-}$ and *ApoE*$^{-/-}$*miR-21*$^{-/-}$ mice, but less stable (larger necrotic core) in the latter. Using BMT, we found that the protection conferred in absence of miR-21, in early atherosclerosis, was related to the hematopoietic compartment. Our interpretation is that the absence of miR-21, concomitant limitation of monocyte-derived macrophage influx in the forming lesion and increased apoptosis of local macrophages protected against early atherosclerosis formation. The loss of protection in more advanced stages is most likely due to excessive inflammatory apoptosis due to impaired efferocytosis, and to a possible minor recruitment of NC-Mo in lesions under conditions of prolonged HFD. In a recent study using BMT, Canfran-Duque et al. found that miR21 deficiency in hematopoietic cells accelerated atherosclerosis via increased apoptosis and decreased efferocytosis of plaque macrophages[17] in *LDLr*$^{-/-}$ mice under HFD during 12 weeks. Our results in *ApoE*$^{-/-}$ mice under HFD are mostly in line with those results. The reason why we observed a protection against early atherosclerosis might be due to the decreased level of circulating NC-Mo observed in our model, which likely limited the early accumulation of macrophages in the plaque and therefore delayed the inflammatory effect of unbalanced apoptosis/efferocytosis in the absence of miR21. Surprisingly, a more recent study reported increased lesion size in the thoracic aorta of *miR-21*$^{-/-}$ *ApoE*$^{-/-}$ mice on chow diet [20], which contrasts with our present findings. One unexplained result from that study[20] is that 16 week-old *ApoE*$^{-/-}$ mice had no detectable atherosclerotic lesions in the thoracic aorta.

Our observation that miR-21 controls the survival of NC-Mo are important for several reasons. First, considering that monocyte subsets are committed to divergent functions, there is a need to identify specific factors that regulate the balance between C-Mo and NC-Mo in pathophysiological conditions. Recently, miR-146a was identified as a specific regulator of C-Mo responses during

inflammatory challenges, without NC-Mo modifications[25]. Targeting miR-146 and miR-21 may then serve to limit the expansion and function of selective monocyte subsets. Second, human studies have underscored the relevance of studying monocyte subsets because an imbalance in their relative proportion is linked to several diseases[26]. For instance, increased proportions of NC-Mo have been reported in patients with inflammatory conditions, including sepsis and rheumatoid arthritis[27-29]. In atherosclerosis, the function, as well as time course and spatial distribution of NC-Mo are still unclear. In a previous study in *ApoE*$^{-/-}$ mice on chow diet for 25 weeks, we found that NC-Mo may significantly contribute to lesion formation, at least under moderate hypercholesterolemia[1]. Our current work in *ApoE*$^{-/-}$ mice on chow and high fat diet supports this finding. A recent study suggested an anti-atherogenic role of NC-Mo under massive hypercholesterolemia, in *ldlr*$^{-/-}$ mice under HFD for 15 weeks[8]. The properties and functions of NC-Mo may then differ according to the experimental settings and may account for the discrepancies between our work and that of Canfran-Duque et al[17].
The fact that miR-21 expression increases in NC-Mo could explain their longer longevity as compared to C-Mo. The mechanisms whereby miR-21 regulates the cell death effector pathways in NC-Mo and whether hypercholesterolemia dictates the longevity of NC-Mo through the increase of miR-21 expression need further investigation. We did not find any effect of miR-21 deficiency on monocyte migration despite the decrease in CX3CR1 expression. We cannot exclude a role of miR-21 on NC-Mo patrolling in large arteries, even though this property was shown to be CX3CR1 independent[7, 8]. It is also unlikely that miR-21 deficiency has altered NC-Mo production as it is now well accepted that NC-Mo monocytes derive directly from the C-Mo[30,31, 32]. Yet, we cannot rule out the possibility that the conversion of C-Mo into NC-Mo in blood was partially altered since C-Mo count in blood was unchanged despite a reduction of C-Mo in the bone marrow. Finally, we have not addressed the potential contribution of miR-21 to atherosclerosis through other cell types, particularly T lymphocyte activation[33] and smooth muscle cell proliferation [20, 34].

In summary, the data herein shed light on a previously unknown role of miR-21 in the homeostasis of NC-Mo in *ApoE*$^{-/-}$ mice and brings new evidence on the role of miR-21 in atherosclerosis development.

Acknowledgments, Sources of Funding, & Disclosures
Ackowledgments
We thank Pr Marc E. Rothenberg for kind providing of *miR-21*$^{-/-}$ mice.

Source of funding
This work was supported by Institut National de la Santé et de la Recherche Médicale.
Disclosures
No conflicts of interests to be listed

References

1. Combadiere C, Potteaux S, Rodero M, Simon T, Pezard A, Esposito B, Merval R, Proudfoot A, Tedgui A and Mallat Z. Combined inhibition of CCL2, CX3CR1, and CCR5 abrogates Ly6C(hi) and Ly6C(lo) monocytosis and almost abolishes atherosclerosis in hypercholesterolemic mice. *Circulation*. 2008;117:1649-57.
2. Soehnlein O and Swirski FK. Hypercholesterolemia links hematopoiesis with atherosclerosis. *Trends Endocrinol Metab*. 2013;24:129-36.
3. Smith JD, Trogan E, Ginsberg M, Grigaux C, Tian J and Miyata M. Decreased atherosclerosis in mice deficient in both macrophage colony-stimulating factor (op) and apolipoprotein E. *Proc Natl Acad Sci U S A*. 1995;92:8264-8.
4. Gautier EL, Huby T, Witztum JL, Ouzilleau B, Miller ER, Saint-Charles F, Aucouturier P, Chapman MJ and Lesnik P. Macrophage apoptosis exerts divergent effects on atherogenesis as a function of lesion stage. *Circulation*. 2009;119:1795-804.
5. Swirski FK, Libby P, Aikawa E, Alcaide P, Luscinskas FW, Weissleder R and Pittet MJ. Ly-6Chi monocytes dominate hypercholesterolemia-associated monocytosis and give rise to macrophages in atheromata. *J Clin Invest*. 2007;117:195-205.
6. Auffray C, Fogg D, Garfa M, Elain G, Join-Lambert O, Kayal S, Sarnacki S, Cumano A, Lauvau G and Geissmann F. Monitoring of blood vessels and tissues by a population of monocytes with patrolling behavior. *Science*. 2007;317:666-70.
7. Quintar A, McArdle S, Wolf D, Marki A, Ehinger E, Vassallo M, Miller J, Mikulski Z, Ley K and Buscher K. Endothelial Protective Monocyte Patrolling in Large Arteries Intensified by Western Diet and Atherosclerosis. *Circ Res*. 2017;120:1789-1799.
8. Marcovecchio PM, Thomas GD, Mikulski Z, Ehinger E, Mueller KAL, Blatchley A, Wu R, Miller YI, Nguyen AT, Taylor AM, McNamara CA, Ley K and Hedrick CC. Scavenger Receptor CD36 Directs Nonclassical Monocyte Patrolling Along the Endothelium During Early Atherogenesis. *Arterioscler Thromb Vasc Biol*. 2017;37:2043-2052.
9. Hanna RN, Shaked I, Hubbeling HG, Punt JA, Wu R, Herrley E, Zaugg C, Pei H, Geissmann F, Ley K and Hedrick CC. NR4A1 (Nur77) Deletion Polarizes Macrophages Toward an Inflammatory Phenotype and Increases Atherosclerosis. *Circ Res*. 2011.
10. Chao LC, Soto E, Hong C, Ito A, Pei L, Chawla A, Conneely OM, Tangirala RK, Evans RM and Tontonoz P. Bone marrow NR4A expression is not a dominant factor in the development of atherosclerosis or macrophage polarization in mice. *J Lipid Res*. 2013;54:806-15.
11. Combadiere C, Potteaux S, Gao JL, Esposito B, Casanova S, Lee EJ, Debre P, Tedgui A, Murphy PM and Mallat Z. Decreased atherosclerotic lesion formation in CX3CR1/apolipoprotein E double knockout mice. *Circulation*. 2003;107:1009-16.
12. Gautier EL, Jakubzick C and Randolph GJ. Regulation of the migration and survival of monocyte subsets by chemokine receptors and its relevance to atherosclerosis. *Arterioscler Thromb Vasc Biol*. 2009;29:1412-8.
13. Loyer X, Mallat Z, Boulanger CM and Tedgui A. MicroRNAs as therapeutic targets in atherosclerosis. *Expert Opin Ther Targets*. 2015;19:489-96.
14. Lu TX, Munitz A and Rothenberg ME. MicroRNA-21 is up-regulated in allergic airway inflammation and regulates IL-12p35 expression. *J Immunol*. 2009;182:4994-5002.
15. Sheedy FJ. Turning 21: Induction of miR-21 as a Key Switch in the Inflammatory Response. *Front Immunol*. 2015;6:19.

16. Lu TX, Hartner J, Lim EJ, Fabry V, Mingler MK, Cole ET, Orkin SH, Aronow BJ and Rothenberg ME. MicroRNA-21 limits in vivo immune response-mediated activation of the IL-12/IFN-gamma pathway, Th1 polarization, and the severity of delayed-type hypersensitivity. *J Immunol*. 2011;187:3362-73.
17. Canfran-Duque A, Rotllan N, Zhang X, Fernandez-Fuertes M, Ramirez-Hidalgo C, Araldi E, Daimiel L, Busto R, Fernandez-Hernando C and Suarez Y. Macrophage deficiency of miR-21 promotes apoptosis, plaque necrosis, and vascular inflammation during atherogenesis. *EMBO Mol Med*. 2017;9:1244-1262.
18. Robinet P, Milewicz DM, Cassis LA, Leeper NJ, Lu HS and Smith JD. Consideration of Sex Differences in Design and Reporting of Experimental Arterial Pathology Studies-Statement From ATVB Council. *Arterioscler Thromb Vasc Biol*. 2018;38:292-303.
19. Caligiuri G, Nicoletti A, Zhou X, Tornberg I and Hansson GK. Effects of sex and age on atherosclerosis and autoimmunity in apoE-deficient mice. *Atherosclerosis*. 1999;145:301-8.
20. Jin H, Li DY, Chernogubova E, Sun C, Busch A, Eken SM, Saliba-Gustafsson P, Winter H, Winski G, Raaz U, Schellinger IN, Simon N, Hegenloh R, Matic LP, Jagodic M, Ehrenborg E, Pelisek J, Eckstein HH, Hedin U, Backlund A and Maegdefessel L. Local Delivery of miR-21 Stabilizes Fibrous Caps in Vulnerable Atherosclerotic Lesions. *Mol Ther*. 2018;26:1040-1055.
21. Schaefer A, Jung M, Miller K, Lein M, Kristiansen G, Erbersdobler A and Jung K. Suitable reference genes for relative quantification of miRNA expression in prostate cancer. *Exp Mol Med*. 2010;42:749-58.
22. Joffre J, Potteaux S, Zeboudj L, Loyer X, Boufenzer A, Laurans L, Esposito B, Vandestienne M, de Jager SC, Henique C, Zlatanova I, Taleb S, Bruneval P, Tedgui A, Mallat Z, Gibot S and Ait-Oufella H. Genetic and Pharmacological Inhibition of TREM-1 Limits the Development of Experimental Atherosclerosis. *J Am Coll Cardiol*. 2016;68:2776-2793.
23. Daugherty A, Tall AR, Daemen M, Falk E, Fisher EA, Garcia-Cardena G, Lusis AJ, Owens AP, 3rd, Rosenfeld ME and Virmani R. Recommendation on Design, Execution, and Reporting of Animal Atherosclerosis Studies: A Scientific Statement From the American Heart Association. *Arterioscler Thromb Vasc Biol*. 2017;37:e131-e157.
24. Potteaux S, Gautier EL, Hutchison SB, van Rooijen N, Rader DJ, Thomas MJ, Sorci-Thomas MG and Randolph GJ. Suppressed monocyte recruitment drives macrophage removal from atherosclerotic plaques of Apoe-/- mice during disease regression. *J Clin Invest*. 2011;121:2025-36.
25. Etzrodt M, Cortez-Retamozo V, Newton A, Zhao J, Ng A, Wildgruber M, Romero P, Wurdinger T, Xavier R, Geissmann F, Meylan E, Nahrendorf M, Swirski FK, Baltimore D, Weissleder R and Pittet MJ. Regulation of monocyte functional heterogeneity by miR-146a and Relb. *Cell Rep*. 2012;1:317-24.
26. Ziegler-Heitbrock L. The CD14+ CD16+ blood monocytes: their role in infection and inflammation. *J Leukoc Biol*. 2007;81:584-92.
27. Sprangers S, de Vries TJ and Everts V. Monocyte Heterogeneity: Consequences for Monocyte-Derived Immune Cells. *J Immunol Res*. 2016;2016:1475435.
28. Kawanaka N, Yamamura M, Aita T, Morita Y, Okamoto A, Kawashima M, Iwahashi M, Ueno A, Ohmoto Y and Makino H. CD14+,CD16+ blood monocytes and joint inflammation in rheumatoid arthritis. *Arthritis Rheum*. 2002;46:2578-86.
29. Fingerle-Rowson G, Auers J, Kreuzer E, Fraunberger P, Blumenstein M and Ziegler-Heitbrock LH. Expansion of CD14+CD16+ monocytes in critically ill cardiac surgery patients. *Inflammation*. 1998;22:367-79.

30. Thomas GD, Hanna RN, Vasudevan NT, Hamers AA, Romanoski CE, McArdle S, Ross KD, Blatchley A, Yoakum D, Hamilton BA, Mikulski Z, Jain MK, Glass CK and Hedrick CC. Deleting an Nr4a1 Super-Enhancer Subdomain Ablates Ly6C(low) Monocytes while Preserving Macrophage Gene Function. *Immunity*. 2016;45:975-987.
31. Yona S, Kim KW, Wolf Y, Mildner A, Varol D, Breker M, Strauss-Ayali D, Viukov S, Guilliams M, Misharin A, Hume DA, Perlman H, Malissen B, Zelzer E and Jung S. Fate mapping reveals origins and dynamics of monocytes and tissue macrophages under homeostasis. *Immunity*. 2013;38:79-91.
32. Mildner A, Schonheit J, Giladi A, David E, Lara-Astiaso D, Lorenzo-Vivas E, Paul F, Chappell-Maor L, Priller J, Leutz A, Amit I and Jung S. Genomic Characterization of Murine Monocytes Reveals C/EBPbeta Transcription Factor Dependence of Ly6C(-) Cells. *Immunity*. 2017;46:849-862 e7.
33. Murugaiyan G, da Cunha AP, Ajay AK, Joller N, Garo LP, Kumaradevan S, Yosef N, Vaidya VS and Weiner HL. MicroRNA-21 promotes Th17 differentiation and mediates experimental autoimmune encephalomyelitis. *J Clin Invest*. 2015;125:1069-80.
34. Albinsson S and Sessa WC. Can microRNAs control vascular smooth muscle phenotypic modulation and the response to injury? *Physiol Genomics*. 2011;43:529-33.

Highlights

- miR-21 expression is high in circulating Ly-6C^{lo} monocytes
- The absence of miR-21 alters the survival and number of circulating Ly-6C^{lo} monocytes in mice
- miR-21 deficiency partially protects *ApoE*$^{-/-}$ mice from early but not advanced atherosclerotic plaque formation

Figure legends

Figure 1: miR-21 controls the survival of non-classical monocytes in *ApoE*$^{-/-}$ mice

A- Percentage and numbers of blood monocyte subsets in *ApoE*$^{-/-}$ and *ApoE*$^{-/-}$*miR-21*$^{-/-}$ mice (flow cytometry, n=8 per group). **B-** *miR-21-5p* expression in blood monocyte subsets. **C-** NR4A1 and CX3CR1 mRNA in blood monocyte subsets (n=4-10 per group). **D-** Amount of Ki67^{+}, BCL-2^{+} and Phospho-P38 MAPK^{+} in NC-Mo in mice (n=4 per group). **E-** Monitoring of NC-Mo survival after labeling with DIL^{+} liposomes in *ApoE*$^{-/-}$ and *ApoE*$^{-/-}$*miR-21*$^{-/-}$ mice *in vivo*. **F-** Experimental design of the chimera experiment (left). Relative proportions of circulating CD45.1 and CD45.2 cells 8 weeks following mixed bone marrow transplantation (right). N=8-9 per group. Mann Whitney non-parametric test was used. $^{*}P<0.05$, $^{**}P<0.01$, $^{***}P<0.001$.

Figure 2: miR-21 deficiency decreases the development of early atherosclerosis in *ApoE*$^{-/-}$ mice

A-D Atherosclerosis quantification in *ApoE*$^{-/-}$ and *ApoE*$^{-/-}$*miR-21*$^{-/-}$ mice on chow diet for 24 weeks. **A**- Plaque size in the aorta and **B**- the aortic root. **C**- Macrophage (MOMA2 staining) and **D**- apoptotic macrophage (TUNEL+) quantification in lesions. **E** Quantification of immunofluorescent staining of MOMA2 and CD206 as markers of M2 macrophages (left), and MOMA2 and iNOS as markers of M1 macrophages in lesions (right). **F**- Analysis of the recruitment of NC-Mo in the aorta of *ApoE*$^{-/-}$ and *ApoE*$^{-/-}$*miR-21*$^{-/-}$ mice. Fluorescent green beads were intravenously injected to label circulating Ly-6C^{lo} monocytes, seven days before flow cytometry analysis on digested aortas. **G**- Efferocytosis of CFSE-labeled apoptotic thymocytes by macrophages in peritoneum of *miR-21*$^{-/-}$ or *miR-21*$^{+/+}$ mice *in vivo*. Gates were set using mice that did not receive CFSE-labeled cells. Representative FACS plots are shown for the 2 groups. **H**- Quantification of plaque size in the aortic sinus of mice on chow diet for 12 weeks after bone marrow transplantation. Mann Whitney non-parametric test was used throughout. $^{*}P<0.05$, $^{**}P<0.01$.

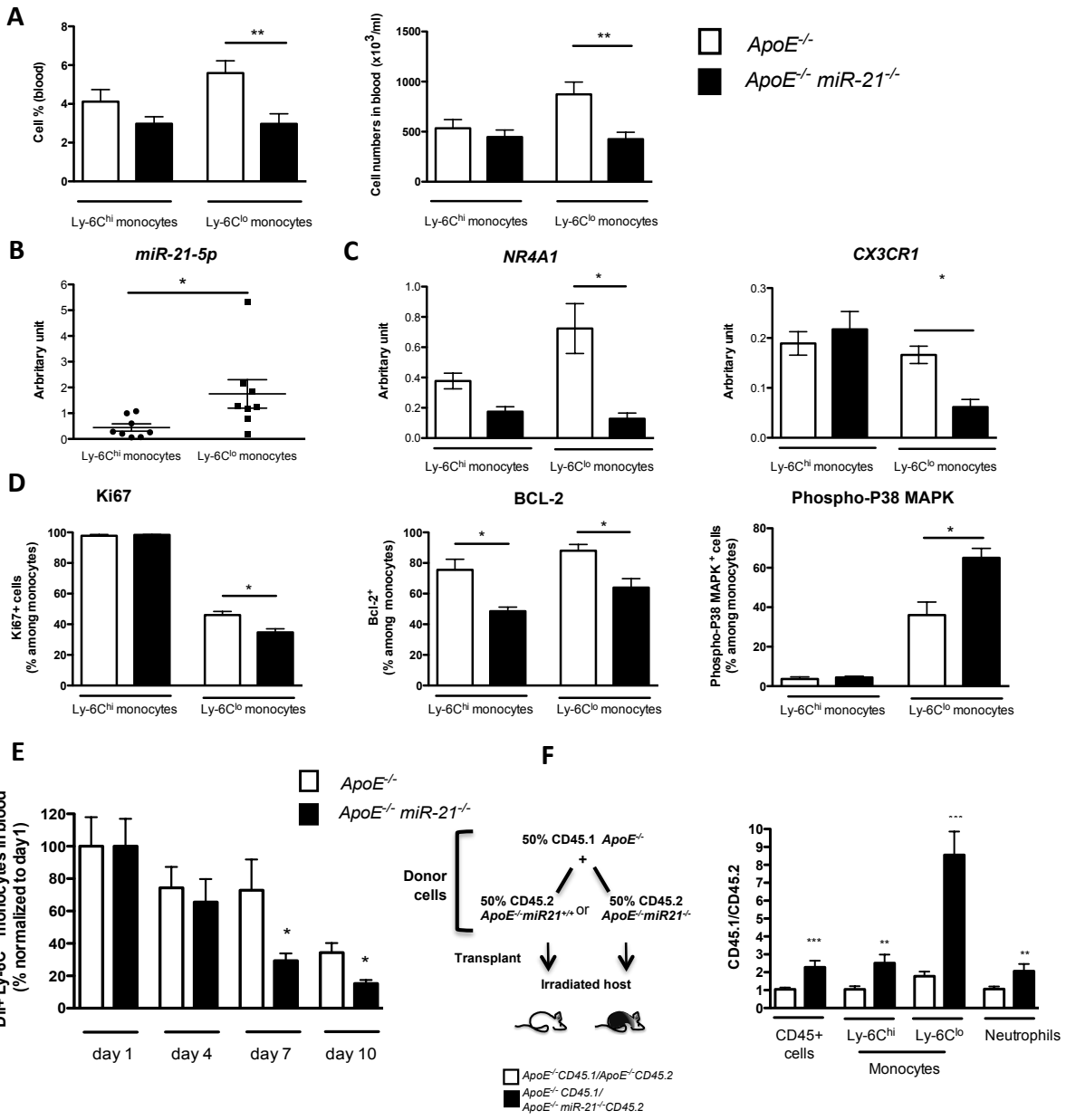
A
Cell % (blood)
Cell numbers in blood (x10^3/ml)
ApoE-/-
ApoE-/- miR-21-/-
Ly-6Chi monocytes
Ly-6Clo monocytes
B
miR-21-5p
Arbritary unit
C
NR4A1
CX3CR1
D
Ki67
Ki67+ cells (% among monocytes)
BCL-2
Bcl-2+ (% among monocytes)
Phospho-P38 MAPK
Phospho-P38 MAPK+ cells (% among monocytes)
E
Dil+ Ly-6Clo monocytes in blood (% normalized to day1)
day 1
day 4
day 7
day 10
F
50% CD45.1 ApoE-/-
Donor cells
50% CD45.2 ApoE-/-miR21+/+ or
50% CD45.2 ApoE-/-miR21-/-
Transplant
Irradiated host
ApoE-/-CD45.1/ApoE-/-CD45.2
ApoE-/- CD45.1/ ApoE-/- miR-21-/-CD45.2
CD45.1/CD45.2
CD45+ cells
Ly-6Chi
Ly-6Clo
Neutrophils
Monocytes

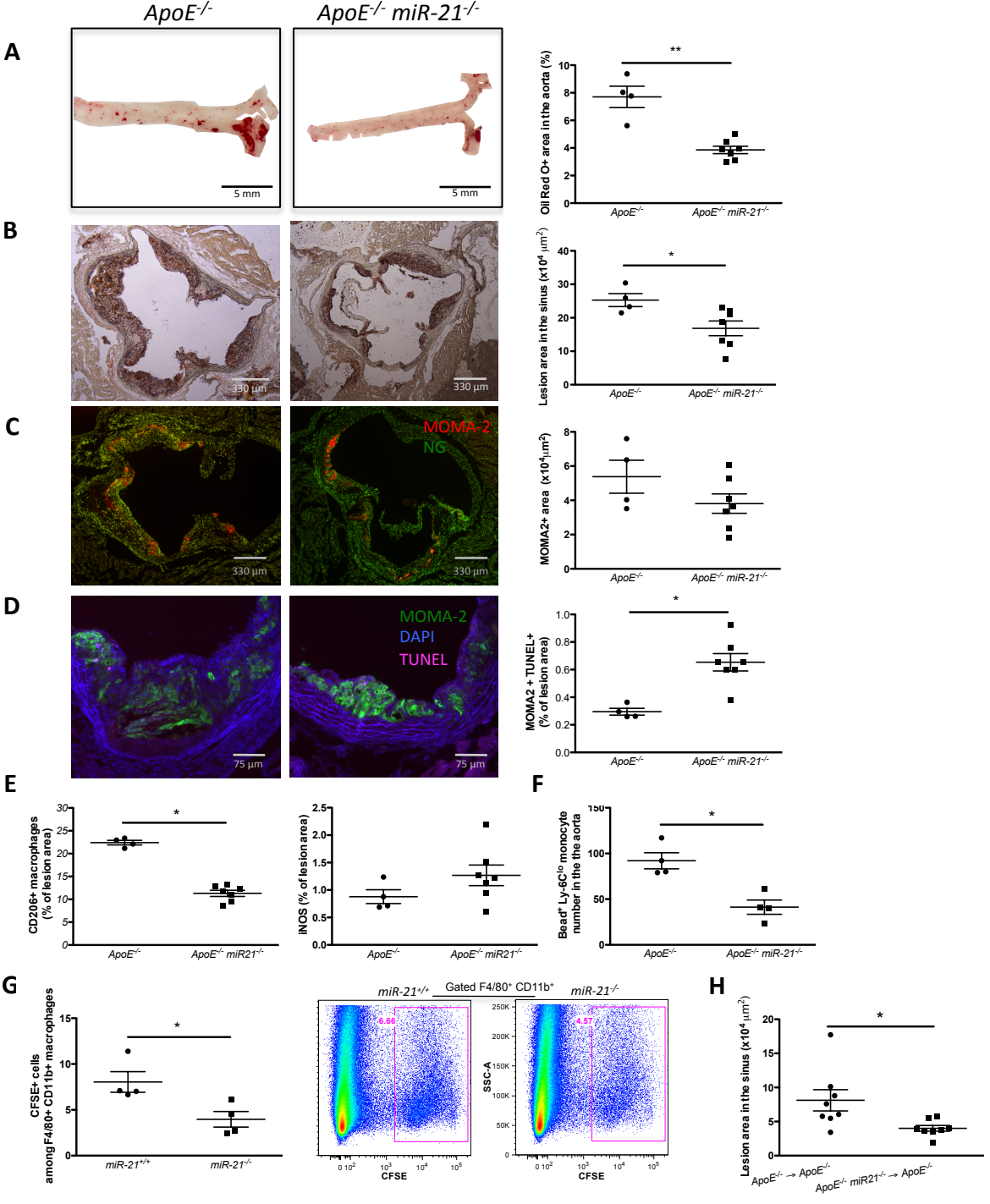
ApoE-/-
ApoE-/- miR-21-/-
A
5 mm
5 mm
Oil Red O+ area in the aorta (%)
**
ApoE-/-
ApoE-/- miR-21-/-
B
330 µm
330 µm
Lesion area in the sinus (x10⁴ µm²)
*
C
MOMA-2
NG
330 µm
330 µm
MOMA2+ area (x10⁴µm²)
D
MOMA-2
DAPI
TUNEL
75 µm
75 µm
MOMA2 + TUNEL+ (% of lesion area)
E
CD206+ macrophages (% of lesion area)
iNOS (% of lesion area)
F
Bead+ Ly-6Clo monocyte number in the the aorta
G
CFSE+ cells among F4/80+ CD11b+ macrophages
miR-21+/+
miR-21-/-
Gated F4/80+ CD11b+
6.66
4.57
SSC-A
CFSE
H
Lesion area in the sinus (x10⁴ µm²)
ApoE-/- → ApoE-/-
ApoE-/- miR21-/- → ApoE-/-

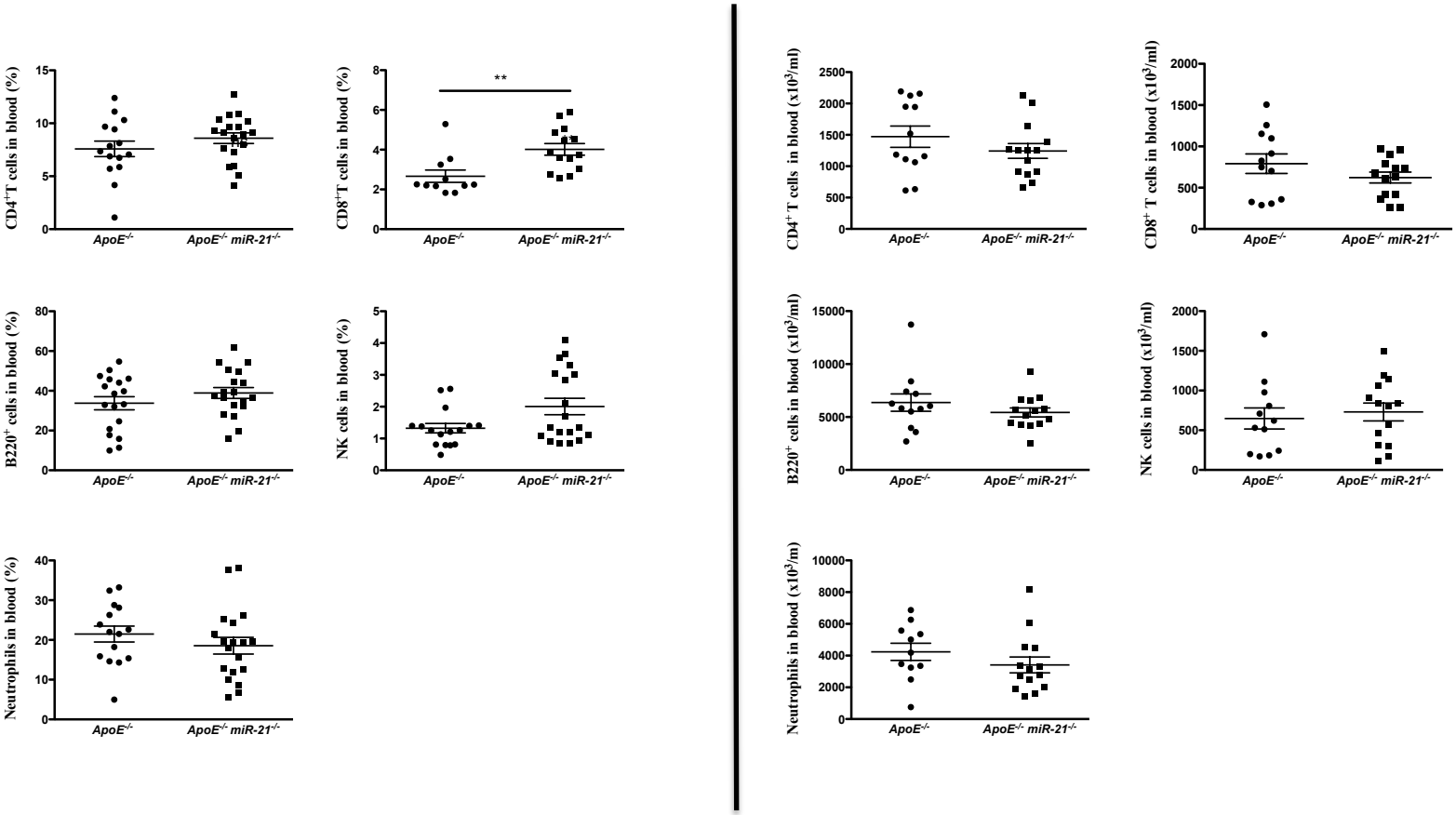

Supplemental figure I

Flow cytometry analysis of blood leukocyte subsets (Left: percentages, right: cell numbers) from *ApoE*$^{-/-}$ and *ApoE*$^{-/-}$ *miR-21*$^{-/-}$ mice on chow diet. Statistical significance was calculated using a Mann Whitney non-parametric test. $^{*}P<0.05$, $^{**}P<0.01$, $^{***}P<0.001$

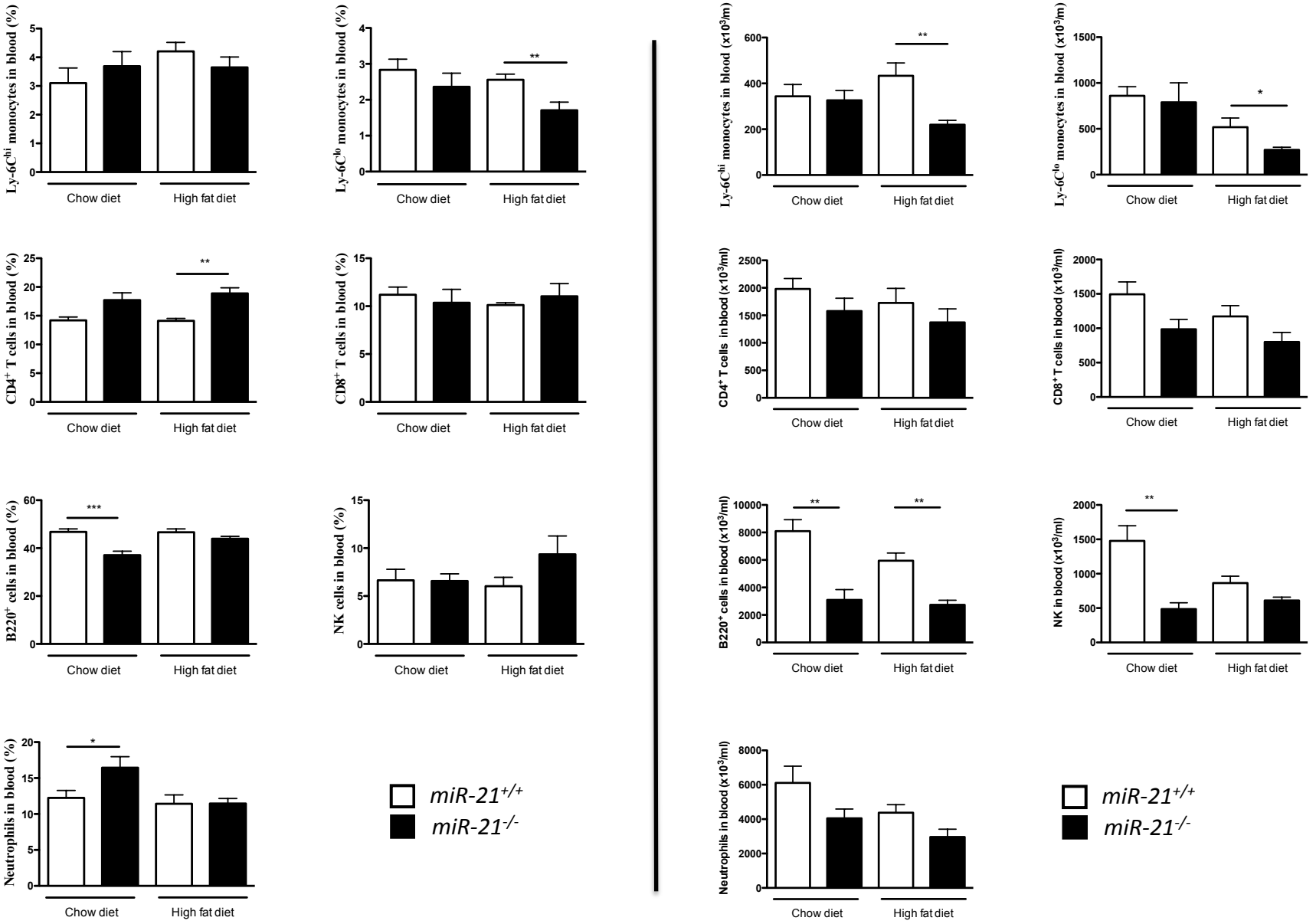

Supplemental figure II

Flow cytometry analysis of blood leukocyte subsets (Left: percentages, right: cell numbers n=5-10 per group) from *miR-21*$^{+/+}$ and *miR-21*$^{-/-}$ mice on chow diet or high fat diet for 2 weeks. Statistical significance was calculated using a Mann Whitney non-parametric test. **P*<0.05, ***P*<0.01, ****P*<0.001

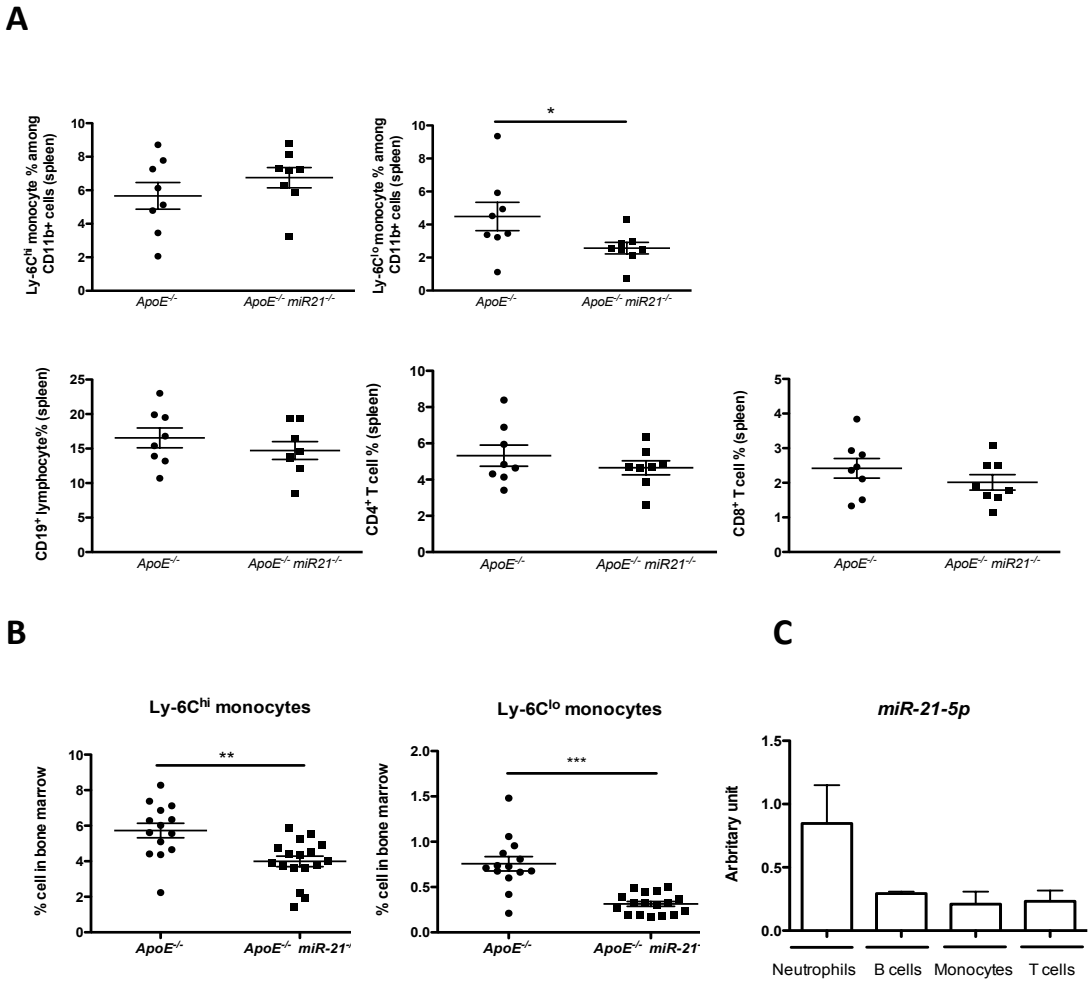

Supplemental figure III

A,B- Flow cytometry analysis of leukocyte subsets in spleen (**A**) and bone marrow (**B**) from *ApoE*$^{-/-}$ and *ApoE*$^{-/-}$*miR-21*$^{-/-}$ mice on chow diet. Statistical significance was calculated using a Mann Whitney non-parametric test. $^{*}P<0.05$, $^{**}P<0.01$, $^{***}P<0.001$ **C-** *miR-21-5p* expression in blood leukocyte subsets from *ApoE*$^{-/-}$ mice on chow diet (n=3 per group). Unpaired two-sided Student's t- test.

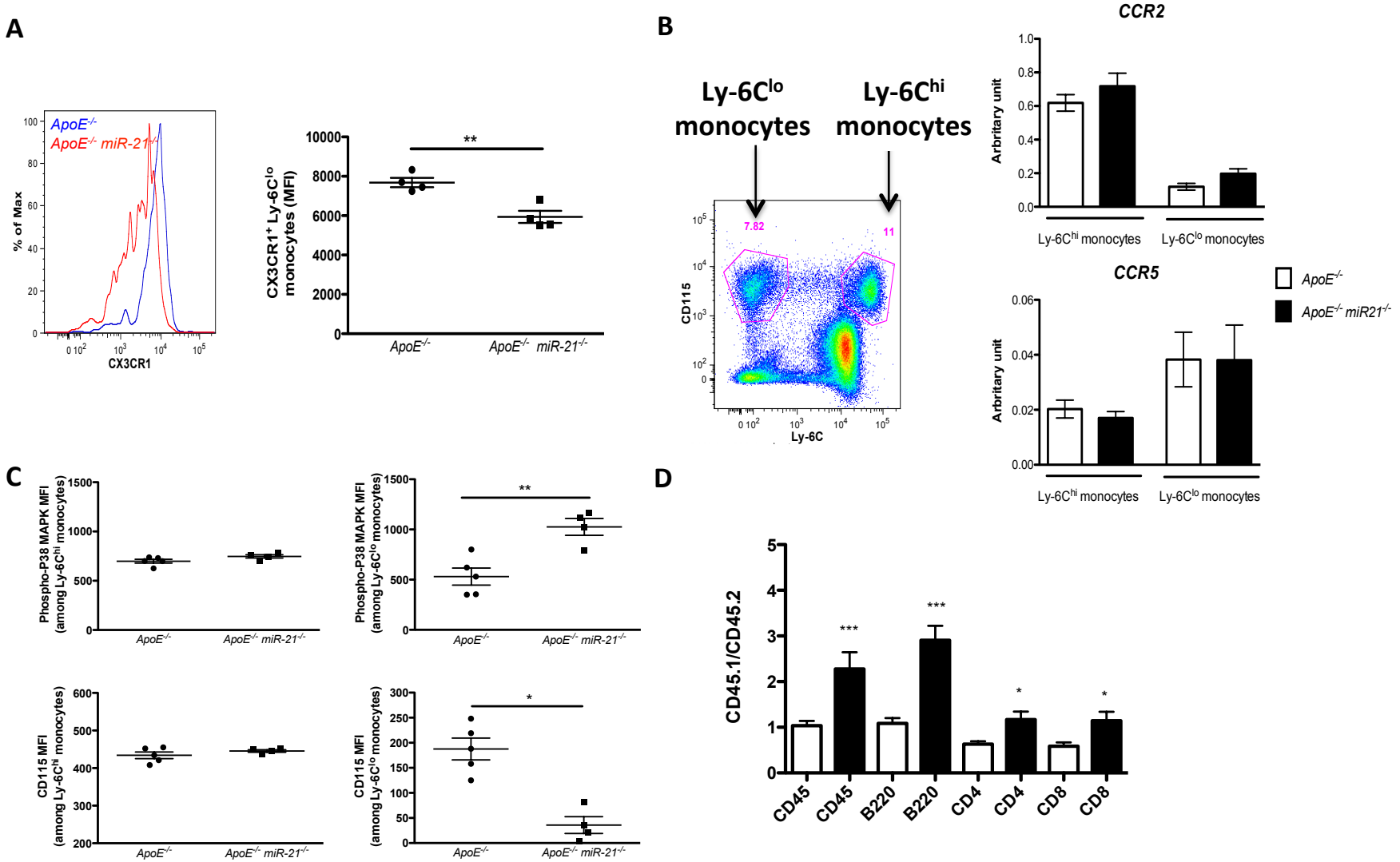

Supplemental figure IV

A- Mean fluorescence intensity of CX3CR1 on splenic NC-Mo. **B-** *Ccr5* and *Ccr2* gene expression in cell sorted C-Mo and NC-Mo from blood of *ApoE*$^{-/-}$ and *ApoE*$^{-/-}$*miR-21*$^{-/-}$ mice (n=4-10 per group). Representative gating strategy (Left) **C-** Phospho-P38 MAPK and CD115 expression as percentages or MFI in monocyte subsets. **D-**Quantification of leukocyte subsets in the blood of chimeric mice 8 weeks after transplantation, by flow cytometry. N=8-9 per group. Statistical significance was calculated using a Mann Whitney non-parametric test. *P<0.05, **P<0.01***P<0.001.

A

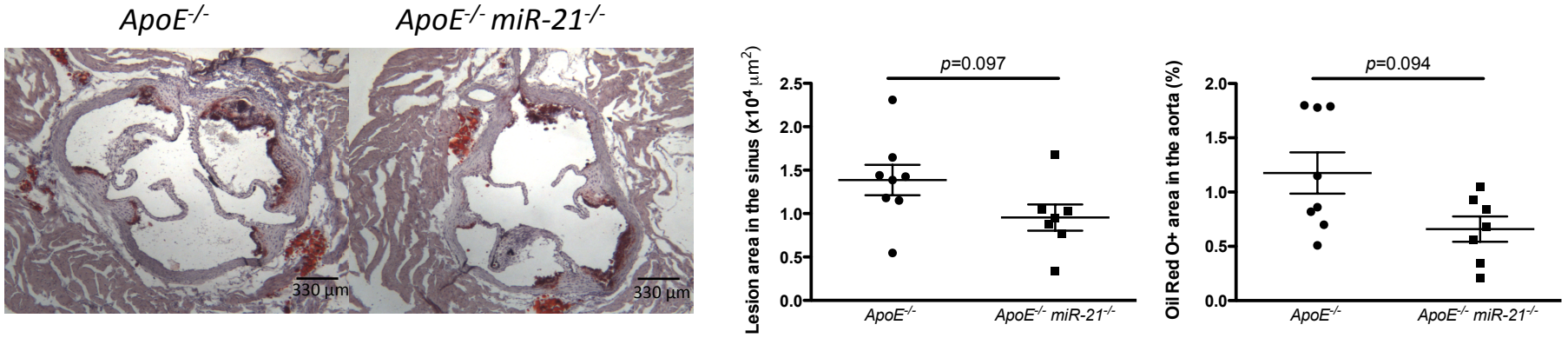

B

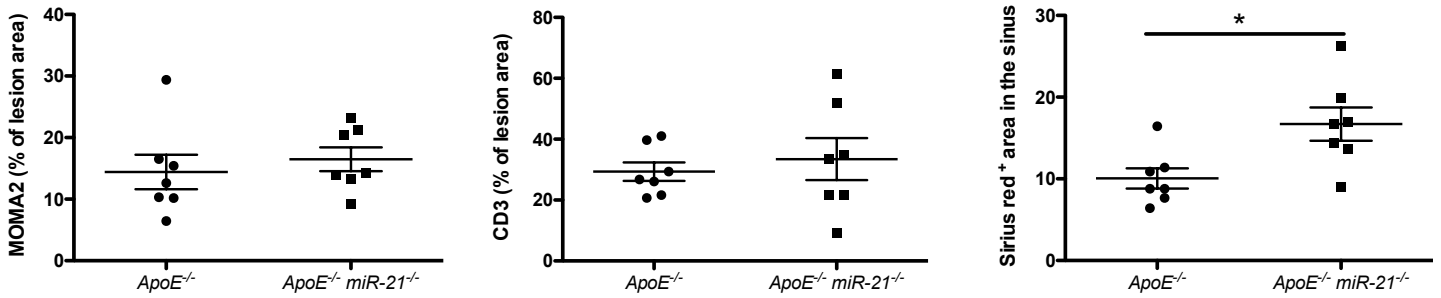

Supplemental figure V

A- Quantification of plaque size in the aortic sinus and in the aorta of *ApoE*$^{-/-}$ and *ApoE*$^{-/-}$*miR-21*$^{-/-}$ on chow diet for 10 weeks. **B-** Quantification of macrophage (MOMA2 staining), T cell (CD3 staining) and collagen (Sirius Red coloration) accumulation per sections of the aortic sinus. Mann Whitney non-parametric test was used. *P<0.05.

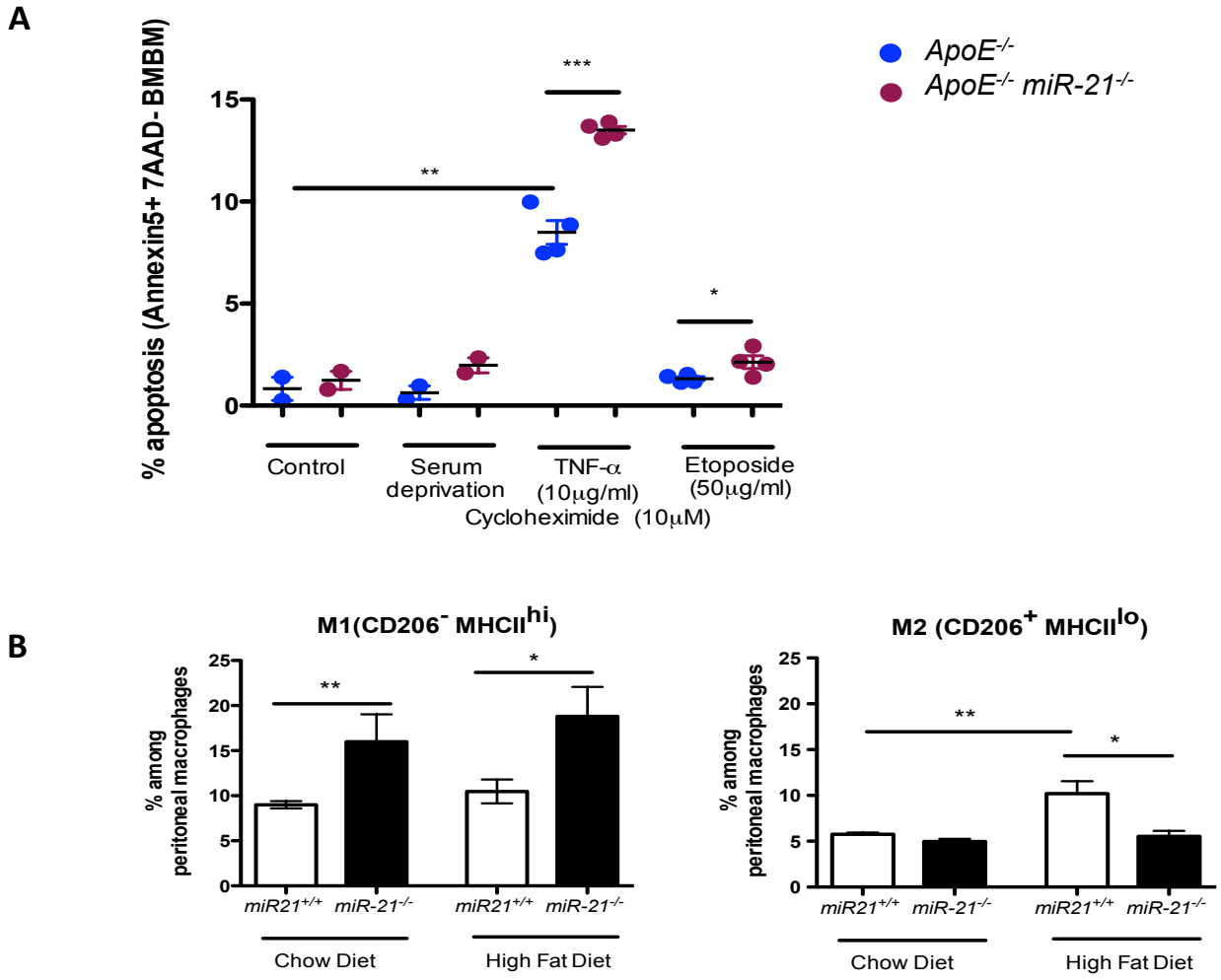

Supplemental figure VI

A-Flow cytometric analysis of apoptotic BMDM from *ApoE*$^{-/-}$ and *ApoE*$^{-/-}$*miR-21*$^{-/-}$ mice after exposure to indicated pro-apoptotic mediators. Unpaired t-test was used. **P*<0.05, ***P*<0.01, ****P*<0.001.

B- Quantification of M1 and M2 macrophages isolated from the inflamed peritoneum after 48 of thioglycollate in *miR-21*$^{+/+}$ and *miR-21*$^{-/-}$ mice on chow or on HFD for two weeks (flow cytometry, n=5 per group). Mann Whitney non-parametric test. **P*<0.05, ***P*<0.01.

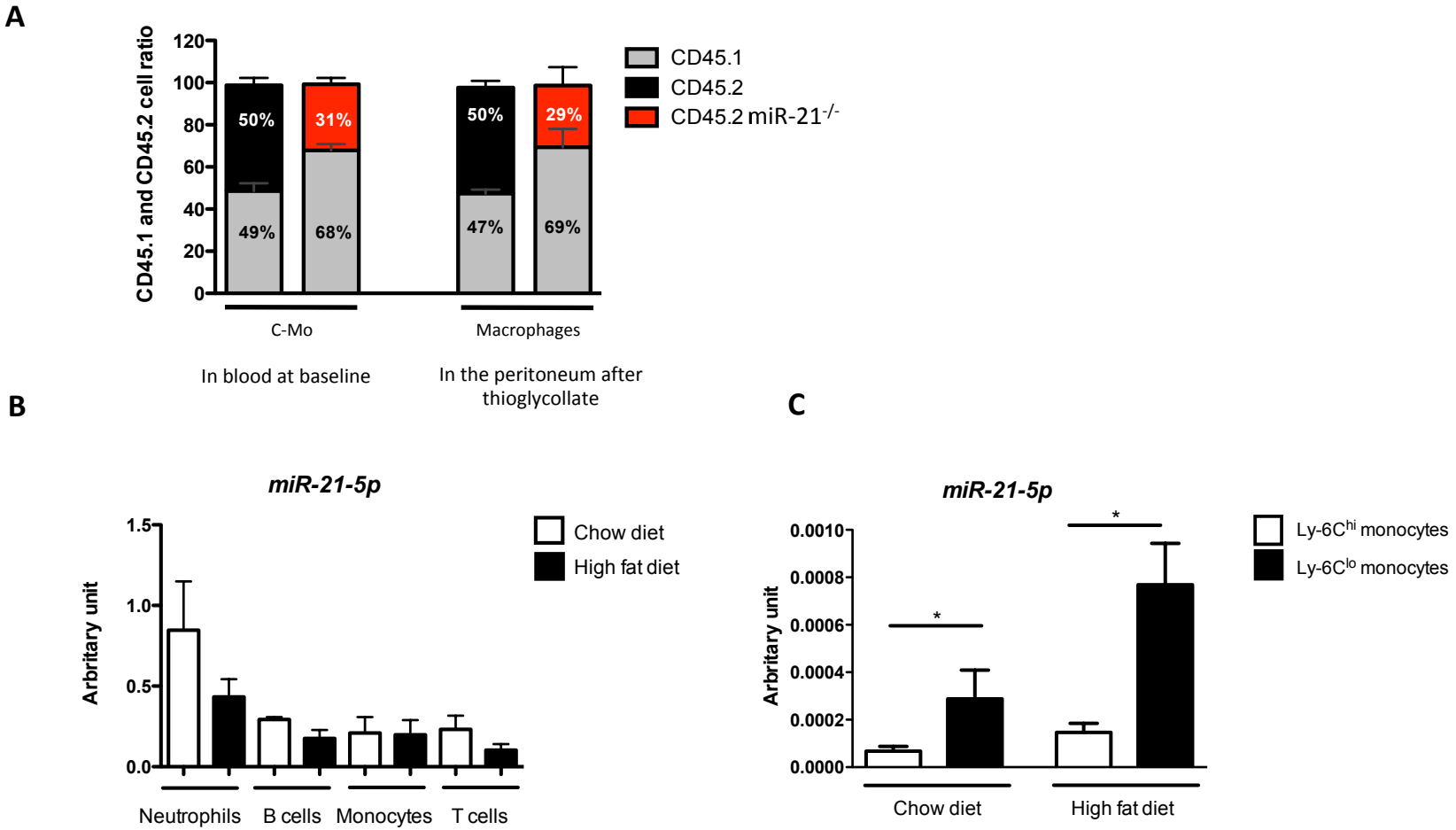

Supplemental figure VII

A- C-Mo migration was evaluated in sterile peritonitis in mixed chimera mice (Experimental design as in Fig1G). The chimerism of C-Mo was tested in both groups in blood before thioglycollate injection. Five days after thioglycollate injection, the relative proportions of CD45.1 and CD45.2 monocyte-derived macrophages was quantified in the peritoneal cavity. N=4-5 per group. **B-** *miR-21-5p* expression in circulating leukocyte subsets from *ApoE*$^{-/-}$ mice on chow diet (as in Supl fig 3C) or high fat diet for 2 weeks (n=4 per group). **C-** *miR-21-5p* expression in blood monocyte subsets from *ApoE*$^{-/-}$ mice on chow or high fat diet for 2 weeks (n=8 per group)

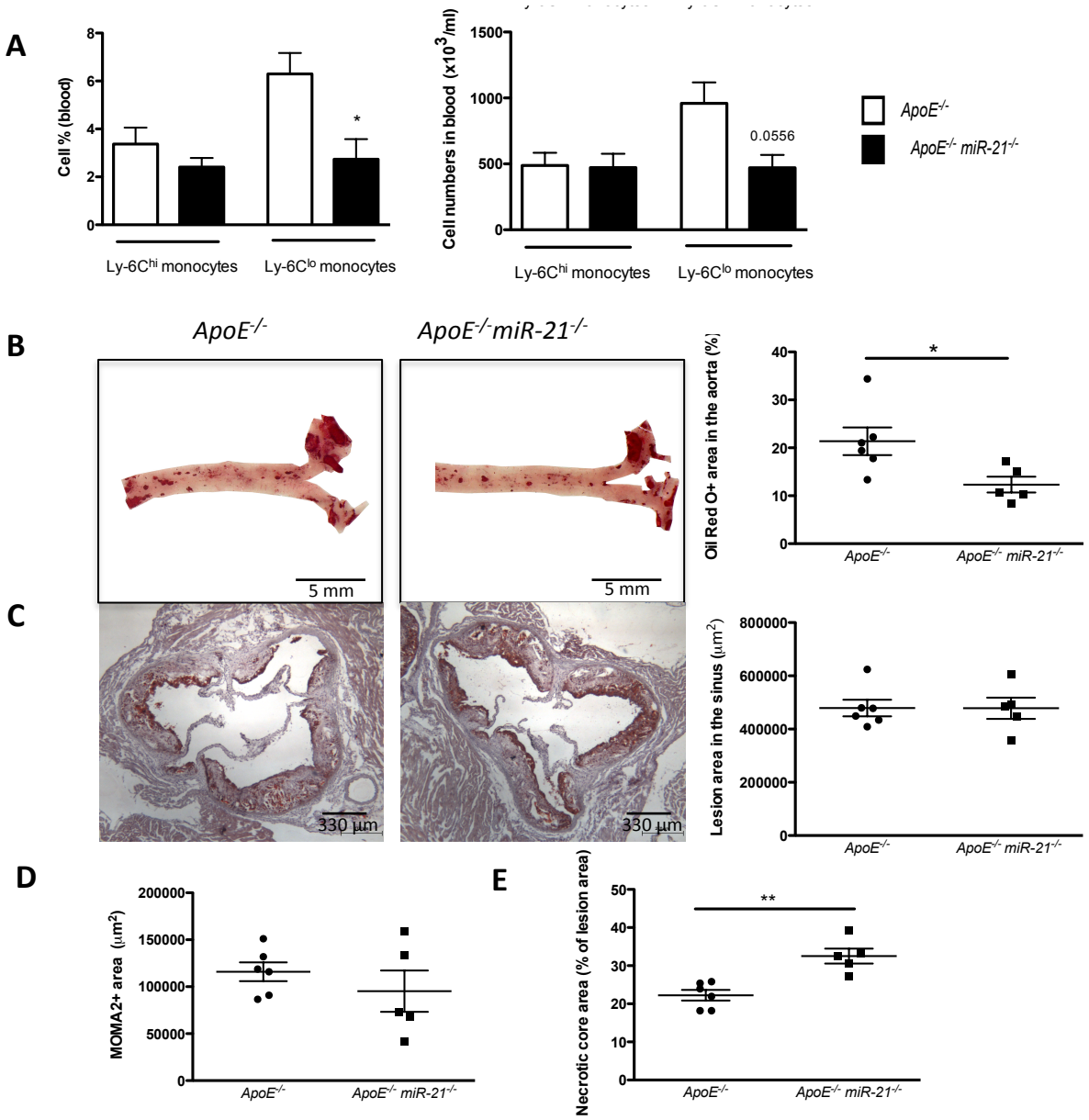

Supplemental figure VIII

A- Analysis of monocyte subset amount and number in *ApoE*$^{-/-}$ and *ApoE*$^{-/-}$*miR-21*$^{-/-}$ mice under HFD for 10 weeks (n=5/ group)**B-C** Atherosclerosis quantification in mice on HFD for 10 weeks. **B-** Plaque size in the aorta and **C-** in the aortic root. **D-** Quantification of macrophage accumulation and **E-** necrotic core area in lesions of the 2 groups. Statistical significance was calculated using a Mann Whitney non-parametric test. *P<0.05, **P<0.01.

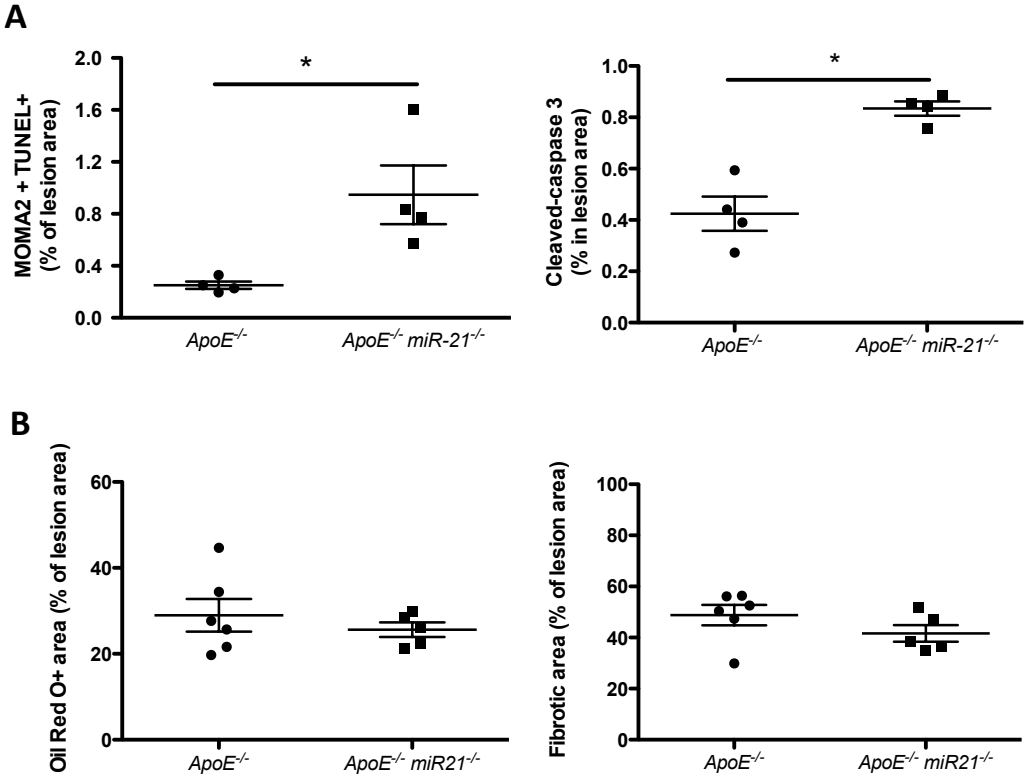

Supplemental figure IX

ApoE$^{-/-}$ and *ApoE*$^{-/-}$*miR-21*$^{-/-}$ mice under HFD for 10 weeks **A-** Quantification of apoptotic macrophages with TUNEL and cleaved-caspase 3 stainings in plaques. **B-** Quantification of lipid^{+} (Oil Red O^{+} area) and collagen^{+} (Sirius Red^{+}) areas within the lesions in the aortic sinus of mice. Statistical significance was calculated using a Mann Whitney non-parametric test. *$P<0.05$.

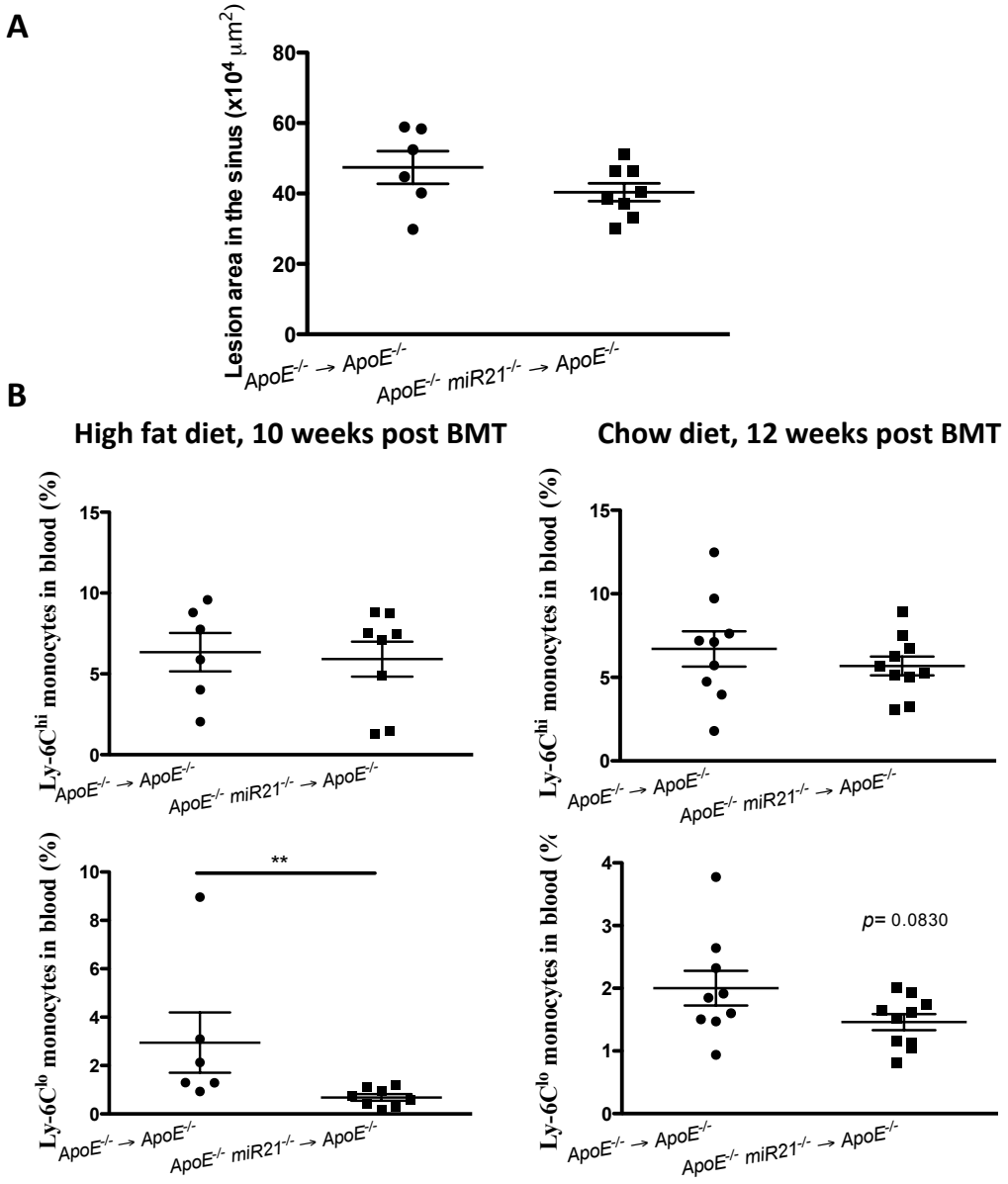

Supplemental figure X

A- Quantification of plaque size in the aortic sinus of mice on HFD for 10 weeks after BMT **B-** Monocyte susbets in blood of mice. Mann Whitney non-parametric test was used. *P<0.05.